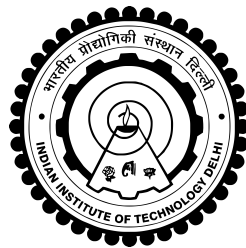


**RF FRONT-ENDS FOR ASYNCHRONOUS
TRANSCEIVERS**

ATUL THAKUR



**DEPARTMENT OF ELECTRICAL ENGINEERING
INDIAN INSTITUTE OF TECHNOLOGY DELHI
MARCH, 2021**

©Indian Institute of Technology Delhi (IITD), New Delhi, 2021

RF FRONT-ENDS FOR ASYNCHRONOUS TRANSCEIVERS

by

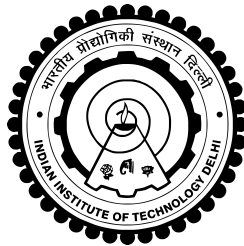
Atul Thakur

Department of Electrical Engineering

Submitted

in fulfillment of the requirements of the degree of Doctor of Philosophy

to the



INDIAN INSTITUTE OF TECHNOLOGY DELHI

MARCH, 2021

To my loving *mother* ...

Certificate

This is to certify that the thesis entitled “**RF Front-Ends for Asynchronous Transceivers**”, being submitted by **Mr. Atul Thakur** for the award of the degree of **Doctor of Philosophy** to the Department of Electrical Engineering, Indian Institute of Technology Delhi, is a record of bonafide work done by him under my supervision and guidance. The matter embodied in this thesis has not been submitted to any other University or Institute for the award of any other degree or diploma.

Shouri Chatterjee

Professor,
Department of Electrical Engineering,
Indian Institute of Technology Delhi,
Hauz Khas, New Delhi - 110016,
INDIA.

Acknowledgements

I would like to express my deepest gratitude to my supervisor Professor Shouri Chatterjee for his guidance, support and encouragement. I am very grateful for giving an opportunity to work with him.

My special thanks to Professor Shankar Prakriya, Professor Ananjan Basu and Professor Swades De, members of my research committee for all their support.

Special thanks to Roohie Kaushik, Sanjeev Kumar, Supriya Chakroborty, Sweta Agarwal, Akash Jain, Rajib Ghosh, Rohit, Nitin, Sarvesh, Jassi, Satya Bairagi and Ajay who increased my desire to pursue PhD studies. The UG students, Parv Aggarwal and Tanay who helped me in different ways. My thanks to Ashish T.R, Sarita, Swapna, Athar Kamal and Dyuti with whom I had many technical discussions.

I am grateful to the Department of Electrical Engineering at the Indian Institute of Technology Delhi for providing me the facilities. I would specially like to mention the help which Mr. Rakesh Kumar, Mr. Satish and Mr. Yatindra have provided me during my research work.

My deepest gratitude to my mother, father, and sister for their love. Thanks to my wife Dr. Priyanka Thakur, for her patience, love and support.

Finally, I acknowledge all other who have helped me and whose names could not be accommodated in this brief acknowledgement.

Atul Thakur

Abstract

Wireless Sensor Networks (WSN) covers the broad area of applications that may be bio-medically inspired, commercially inspired, or maybe needed for military applications. Specifically, the bio-medically inspired body-area WSN have a fundamental requirement of low power consumption, moderate data rate, and microscopic volume. For applications like capsule endoscopy, intra-ocular transmitters, pacemakers, and neural recorders, the entire system is to be packaged with minimal volume. As such, in such applications, there is no room for a discrete crystal oscillator. Also, minimum power should be consumed during the data transmission to maintain the communication link for a more prolonged period until capsule travels entirely through the large and the small intestine, which takes approximately 24 hours. However, a moderate to high data rate is required to maintain the picture quality. These specifications are mostly dictated by the application leading to the specific transceiver architecture design.

In all most every synchronous transceiver architecture design, a crystal oscillator is pre-requisite, which provides the time definition to the transceiver. On the other hand, the on-chip oscillator can not provide precise and accurate timing information due to the process-voltage-temperature (PVT) variations. The frequency of an on-chip oscillator can vary up to 15%, which can be controlled using off-chip calibration. In contrast, crystal oscillator frequency variation is typically $< 0.005\%$, which accounts for $< 50\text{ppm}$. Crystal oscillators have quality factor (Q) in the range $10^4 - 10^6$. External passive and active temperature compensation and control can lead to temperature coefficient under $1\text{ppm}/^\circ\text{C}$.

These merits of crystal oscillator comes with the additional cost and increased power budget. To upconvert the crystal frequency up to the Nyquist rate and to make it temperature stable, dedicated on-chip circuits are required. Hence, with the asynchronous transceiver design, which is the transceiver without the crystal oscillator, there is the possibility to improve the margin over power consumption, cost and ultimately could lead to complete SoC design.

For the bio-medical application like capsule-endoscopy, a new code-based frequency-detection asynchronous transceiver architecture is modeled and analyzed on Simulink Matlab. The transceiver uses the OOK modulation, and OOK is opted to save the transmission power as, during the low-bit interval of the data, zero power is transmitted. Band of frequencies ranging from 400-500 MHz shows minimum attenuation as projected by the human body model. Hence, a 450 MHz carrier with a 1 Mbps data rate is chosen for transmission. The clock and data recovery circuit used in the model can lock onto the frequency and recover data and clock correctly.

For the actual implementation of the transceiver on-chip, 1.8 GHz oscillator is designed for which new inductors are fabricated, characterized, and their impact on oscillator phase noise is studied. Dividing 1.8 GHz by a factor of four provides the required 450 MHz carrier.

RF front-end of the receiver chain is designed, which has a low noise amplifier (LNA), active balun, and a differential mixer. All these circuits after integration consume more than 20 mW for a 3.1 dB noise figure of the RF front-end. To improve the sensitivity and reduce

the power consumption of the front-end, a new single to differential LNA is proposed. For 1.25 dB of noise figure, LNA consumes only 7.9 mW. Later the passive mixer on top of the same LNA is implemented, which reuses the LNA current. With this topology, the complete front-end design gives 2.5 dB of noise figure for the same power consumption.

To further improve the sensitivity of the RF front-end, a new sub-1 dB noise-figure ESD-safe LNA topology is proposed. The proposed LNA is fabricated in 130 nm CMOS process. The LNA is lab-tested for 2.5 kV HBM ESD zap and has passed the JEDEC standards within a 10% margin of its initial diode characteristics. LNA is characterized for a 0.9 dB noise figure at 900 MHz for 5.2 mW of power consumption. LNA uses a single inductor to achieve input matching and a total of only two passives, thereby saving on the active area requirements.

A hybrid circuit of this very-low noise figure LNA is implemented, which can be switched to the oscillator mode. Therefore, the same circuit is used as an LNA during the reception and as an oscillator during the transmission. This topology is fabricated in the 65 nm CMOS process. The oscillator can directly modulate the data for OOK or FSK transmission and can also drive the 50 Ω antenna. Therefore, the hybrid circuit can work as a complete transceiver because the LNA and the buffer (used as a mixer) can demodulate the carrier during the receiving mode. During the transmission mode, it can be switched to the oscillator mode, and the oscillator is capable of modulating data and driving the antenna. Hence, omitting the need for SPDT-switches as the same circuit can do transmission and reception both in half-duplex mode.

सार

वायरलेस सेंसर नेटवर्क (डब्ल्यूएसएन) अनुप्रयोगों के व्यापक क्षेत्र को कवर करता है जो जैव-चिकित्सकीय रूप से प्रेरित, व्यावसायिक रूप से प्रेरित, या शायद सैन्य अनुप्रयोगों के लिए आवश्यक हो सकते हैं। विशेष रूप से, जैव-चिकित्सकीय रूप से प्रेरित शरीर-क्षेत्र WSN में कम बिजली की खपत, मध्यम डेटा दर और सूक्ष्म मात्रा की मूलभूत आवश्यकता होती है। कैप्सूल एंडोस्कोपी, इंट्रा-ऑक्यूलर ट्रांसमीटर, पेसमेकर और न्यूरल रिकॉर्डर्स जैसे अनुप्रयोगों के लिए, पूरे सिस्टम को न्यूनतम मात्रा के साथ पैक किया जाना है। ऐसे अनुप्रयोगों में, असतत क्रिस्टल थरथरानवाला के लिए कोई जगह नहीं है। इसके अलावा, अधिक लंबी अवधि के लिए संचार लिंक को बनाए रखने के लिए डेटा ट्रांसमिशन के दौरान न्यूनतम शक्ति का उपभोग किया जाना चाहिए जब तक कि कैप्सूल पूरी तरह से बड़ी और छोटी आंत के माध्यम से यात्रा नहीं करता है, जिसमें लगभग 24 घंटे लगते हैं। हालांकि, तस्वीर की गुणवत्ता बनाए रखने के लिए एक मध्यम से उच्च डेटा दर की आवश्यकता होती है। इन विशिष्टताओं को ज्यादातर विशिष्ट ट्रांसीवर वास्तुकला डिजाइन के लिए अग्रणी अनुप्रयोग द्वारा निर्धारित किया जाता है।

सभी समकालिक ट्रांसीवर वास्तुकला डिजाइन में, एक क्रिस्टल थरथरानवाला पूर्व-अपेक्षित है, जो ट्रांसीवर को समय की परिभाषा प्रदान करता है। दूसरी ओर, ऑन-चिप थरथरानवाला प्रक्रिया-वोल्टेज-तापमान (पीवीटी) विविधताओं के कारण सटीक और सटीक समय की जानकारी नहीं दे सकता है। ऑन-चिप थरथरानवाला की आवृत्ति 15% तक भिन्न हो सकती है, जिसे ऑफ-चिप अंशांकन का उपयोग करके नियंत्रित किया जा सकता है। इसके विपरीत, क्रिस्टल थरथरानवाला आवृत्ति भिन्नता आमतौर पर 0.004% है, जो 40 पीपीएम है। क्रिस्टल ऑसिलेटर्स में $10^4 - 10^6$ रेंज में गुणवत्ता कारक (Q) है। बाहरी निष्क्रिय और सक्रिय तापमान मुआवजा और नियंत्रण $1\text{ppm} / ^\circ\text{C}$ के तहत तापमान गुणांक को जन्म दे सकता है। क्रिस्टल थरथरानवाला के ये गुण अतिरिक्त लागत और बढ़े हुए बिजली बजट के साथ आते हैं। Nyquist दर तक क्रिस्टल की आवृत्ति को बढ़ाने और इसे तापमान को स्थिर बनाने के लिए, ऑन-चिप सर्किट को समर्पित करने की आवश्यकता होती है। इसलिए, अतुल्यकालिक ट्रांसीवर डिजाइन के साथ, जो क्रिस्टल थरथरानवाला के बिना ट्रांसीवर है, बिजली की खपत, लागत पर मार्जिन में

सुधार करने की संभावना है और अंततः पूर्ण SoC डिजाइन हो सकता है।

कैप्सूल-एंडोस्कोपी जैसे जैव-चिकित्सा अनुप्रयोग के लिए, एक नया कोड-आधारित फ्रीक्वेंसी-डिटेक्शन एसिं-क्रोनस ट्रांसीवर वास्तुकला मॉडलिंग और सिमुलिक मैटलैब पर विश्लेषण किया गया है। ट्रांसीवर OOK मॉड्यूलेशन का उपयोग करता है, और OOK को ट्रांसमिशन पावर को बचाने के लिए चुना जाता है, जैसे कि डेटा के कम-बिट अंतराल के दौरान, शून्य पावर प्रसारित होता है। 400-500 मेगाहर्ट्ज से आवृत्तियों का बैंड मानव शरीर मॉडल द्वारा अनुमानित न्यूनतम क्षीणन को दर्शाता है। इसलिए, 1 एमबीपीएस डेटा दर के साथ 450 मेगाहर्ट्ज वाहक ट्रांसमिशन के लिए चुना जाता है। मॉडल में उपयोग की जाने वाली घड़ी और डेटा रिकवरी सर्किट आवृत्ति पर लॉक कर सकते हैं और डेटा और घड़ी को ठीक से वसूल कर सकते हैं।

ट्रांसीवर ऑन-चिप के वास्तविक कार्यान्वयन के लिए, 1.8 गीगाहर्ट्ज थरथरानवाला डिजाइन किया गया है, जिसके लिए नए प्रेरकों को गढ़ा, चित्रित किया गया है, और थरथरानवाला चरण शोर पर उनके प्रभाव का अध्ययन किया जाता है। चार के एक कारक द्वारा 1.8 गीगाहर्ट्ज विभाजित करना आवश्यक 450 मेगाहर्ट्ज वाहक प्रदान करता है।

रिसीवर श्रृंखला के आरएफ फ्रंट-एंड को डिजाइन किया गया है, जिसमें कम शोर एम्पलीफायर (एलएनए), सक्रिय बालून और एक अंतर मिक्सर है। एकीकरण के बाद ये सभी सर्किट आरएफ फ्रंट-एंड के 3.1 डीबी शोर आकृति के लिए 20 mW से अधिक खपत करते हैं। संवेदनशीलता को बेहतर बनाने और फ्रंट-एंड की बिजली की खपत को कम करने के लिए, एलएनए से डिफरेंशियल के लिए एक नया सिंगल प्रस्तावित है। शोर के आंकड़े के 1.25 डीबी के लिए, LNA केवल 7.9 mW की खपत करता है। बाद में उसी LNA के शीर्ष पर निष्क्रिय मिक्सर को लागू किया जाता है, जो LNA करंट का पुनः उपयोग करता है। इस टोपोलॉजी के साथ, पूर्ण फ्रंट-एंड डिजाइन समान बिजली की खपत के लिए 2.5 डीबी शोर का आंकड़ा देता है।

आरएफ फ्रंट-एंड की संवेदनशीलता को और बेहतर बनाने के लिए, एक नया सब -1 डीबी शोर-आंकड़ा ईएसडी-सुरक्षित एलएनए टोपोलॉजी प्रस्तावित है। प्रस्तावित LNA 130 एनएम CMOS प्रक्रिया में निर्मित है।

LNA को 2.5 kV HBM ESD जैप के लिए लैब-टेस्ट किया गया है और इसके प्रारंभिक डायोड विशेषताओं के 10 % मार्जिन के भीतर JEDEC मानकों को पारित किया है। LNA को 5.2 मेगावाट बिजली की खपत के लिए 900 मेगाहर्ट्ज पर 0.9 डीबी शोर आकृति के लिए विशेषता है। LNA इनपुट मिलान और कुल दो पैसिव्स को प्राप्त करने के लिए एकल प्रारंभ करनेवाला का उपयोग करता है, जिससे सक्रिय क्षेत्र की आवश्यकताओं पर बचत होती है।

इस बहुत कम शोर वाली आकृति LNA का एक हाइब्रिड सर्किट कार्यान्वित किया जाता है, जिसे ऑसिलेटर मोड में स्विच किया जा सकता है। इसलिए, रिसेप्शन के दौरान और ट्रांसमिशन के दौरान एक थरथरानवाला के रूप में एक ही सर्किट का उपयोग LNA के रूप में किया जाता है। यह टोपोलॉजी 65 एनएम सीएमओएस प्रक्रिया में गढ़ी गई है। थरथरानवाला सीधे OOK या FSK प्रसारण के लिए डेटा को नियंत्रित कर सकता है और 50 *Omega* एंटीना ड्राइव भी कर सकता है। इसलिए, हाइब्रिड सर्किट एक पूर्ण ट्रांसीवर के रूप में काम कर सकता है क्योंकि LNA और बफर (मिक्सर के रूप में उपयोग किया जाता है) प्राप्त मोड के दौरान वाहक को ध्वस्त कर सकता है। ट्रांसमिशन मोड के दौरान, इसे ऑसिलेटर मोड में स्विच किया जा सकता है, और ऑसिलेटर डेटा को मॉड्यूलेट करने और एंटीना को चलाने में सक्षम है। इसलिए, एक ही सर्किट के रूप में SPDT- स्विच की आवश्यकता को छोड़ना आधा-द्वैध मोड में ट्रांसमिशन और रिसेप्शन दोनों कर सकता है।

Table of Contents

	Page
List of Figures	vii
List of Tables	xvi
Chapter 1 Introduction	1
1.1 Need of asynchronous transceivers	2
1.2 Application oriented transceiver modeling	3
1.3 Link budget	4
1.4 Conventional Tx/Rx architectures	5
1.5 Motivation	6
1.6 Proposed transceiver modeling	8
1.7 Transmitter operation	9
1.8 Receiver operation	9
1.9 Code-based frequency-locking algorithm	12
1.10 Simulation results of the proposed transceiver	14

1.10.1	Advantages of the proposed transceiver architecture	16
1.11	Design challenges of the proposed architecture	18
1.12	Conclusion	19
 Chapter 2 Inductor design and its influence on the oscillator (DCO) perfor-		
	mance	21
2.1	Introduction	21
2.2	VCO architectures	22
2.2.1	LC resonator	25
2.2.2	Low power oscillator design	26
2.3	Inductor design review	28
2.3.1	Modelling of inductor	29
2.3.2	Substrate shielding	30
2.3.3	Inductor on-chip interferences	31
2.4	Inductor design and measurements	31
2.4.1	Inductor design	31
2.4.2	Measurements	34
2.4.3	DCO implementation	35
2.5	Conclusion	37
 Chapter 3 Low noise figure RF front-end design		39
3.1	Introduction	39

3.2	Low noise amplifier design	41
3.2.1	Active balun design	42
3.3	Mixer design	43
3.4	Proposed single-to-differential output LNA	46
3.5	Proposed LNA design and analysis	47
3.5.1	IDL Design	48
3.5.2	Impedance matching and power consumption	51
3.5.3	Noise cancellation	52
3.5.4	Differential gain and NF of the LNA	52
3.5.5	Bias Circuit	54
3.5.6	Design of RF-front end	54
3.6	Simulation Results	55
3.7	Conclusion	57
Chapter 4 A 4.4-mA ESD-safe 900-MHz LNA with 0.9 dB noise figure		59
4.1	Introduction	59
4.2	LNA Circuit Analysis	63
4.2.1	Motivation	63
4.2.2	Narrowband input matching for the wideband LNA	65
4.2.3	Gain	67
4.3	NF analysis and improvement	69
4.4	Implementation details	71

4.4.1	Design strategy	71
4.4.2	Modified LNA with improved input matching	72
4.4.3	Supply independent biasing	73
4.4.4	Comparison with the conventional inductively degenerated LNA	74
4.4.5	Modeling of package parasitics	76
4.4.6	ESD Design and layout aspects	77
4.5	Measurements	78
4.6	Conclusion	82
Chapter 5 On the Output Impedance of Integrated LNAs		83
5.1	Introduction	83
5.2	Gain with output matching	85
5.2.1	Gain of a stand-alone LNA	85
5.2.2	Gain with a cascoded common source (CCS) buffer	88
5.2.3	Gain with source follower (SF) buffer	88
5.3	Effect on noise performance of the core LNA	89
5.3.1	CCS noise factor calculations	90
5.3.2	SF noise factor calculations	91
5.4	Limit on S_{22} for unconditional stability	92
5.5	Implementation and measurements	93
5.6	Advantages of the output mismatch	95
5.7	Conclusion	96

Chapter 6	Switched LNA/Oscillator based RF Front-end Design	97
6.1	Introduction	97
6.2	Switched LNA/OSC circuit design	98
6.3	Oscillator mode and transmitter operation	101
6.3.1	Oscillator measurements	102
6.4	Measurement of modulation schemes	103
6.4.1	FSK modulation	103
6.4.2	OOK modulation	105
6.5	LNA mode and receiver operation	106
6.5.1	LNA measurements	107
6.6	Demodulation in LNA mode	113
6.6.1	Proposed on-chip FSK and OOK demodulation scheme	114
6.6.1.1	FSK demodulation	115
6.6.1.2	OOK demodulation	116
6.7	Conclusion	117
Chapter 7	Conclusions and Future Scope	119
7.1	Conclusion	119
7.1.1	Asynchronous transceiver modeling	119
7.1.2	Monolithic inductor design and fabrication	120
7.1.3	RF front-end design	121
7.1.4	A 4.4-mA ESD-safe 900-MHz LNA with 0.9 dB noise figure	123

7.1.5	On the Output Impedance of Integrated LNAs	123
7.1.6	Switched LNA/Oscillator based RF Front-end Design	124
7.2	Future Work	126
7.2.1	Future Work-1: Distributed beam-forming	126
7.2.2	Future Work-2: Improvements	128

Bibliography		130
---------------------	--	------------

List of Figures

1.1	Total transmitting loss in the human body model [1].	3
1.2	Transmitter block diagram for the OOK modulation [2]	4
1.3	Open loop receiver model [3]	6
1.4	Super regenerative oscillator receiver architecture [4]	6
1.5	Proposed code-based frequency-detection heterodyne transceiver architecture.	7
1.6	Simulink model of the proposed code based frequency detection heterodyne transceiver.	8
1.7	Clock and data recovery circuit modeled in Matlab® Simulink®.	10
1.8	Second order loop filter [5] used in the CDR to drive the VCO.	10
1.9	Simulation result showing the CDRs control voltage settling.	12
1.10	Frequency lock signal after the code ‘01110’ is detected two times.	13
1.11	Output of the up-counter which stops counting after code detection and the locks the VCOs frequency.	14
1.12	Receiver input with OOK modulated 450 MHz carrier at -80 dBm power.	15

1.13	Demodulated data at the output of the ED.	16
1.14	Recovered code and the data at the output of CDR.	17
2.1	Commonly used LC oscillator topologies, (a) nMOS cross-coupled oscillator, and (b) push-pull cross coupled oscillator.	23
2.2	Power spectrum of the oscillator.	24
2.3	(a) Equivalent resonator for oscillator (excluding bias current) (b) oscillator resonator with equivalent parallel resistances (c) simplified equivalent RLC resonator.	25
2.4	(a) Equivalent resonator circuit for oscillator excluding bias current and negative resistance (b) differential inductor.	27
2.5	Differentially patterned shield [6] spiral shape inductor.	28
2.6	External magnetic field influence on twisted inductor [7].	30
2.7	Die micrograph of the twisted shape inductor (left) with floating substrate shield and spiral shape inductor (right) with ground-signal-ground (GSG) pads.	32
2.8	Simulation results showing (a) Inductance variation (b) Q-factor variation without shielding.	32
2.9	Simulation results showing (a) Inductance variation (b) Q-factor variation with virtual ground shield.	33
2.10	Measured inductance value and Q-factor of (a) the twisted shape inductor, and (b) the 3-turn spiral shape inductor.	34

2.11	(a) DCO implemented using designed passives. (b) Simulated phase noise of the DCO implemented using twisted shape inductor with floating substrate shield and 3-turn spiral shape inductor without substrate shield.	36
3.1	System block digram of the RF front-end.	39
3.2	Inductor Degenerative LNA Schematic [8].	41
3.3	Schematic of single to differential active balun used after LNA [9].	43
3.4	Simulation results of (a) input matching (S_{11}) after two stage integration, and (b) noise figure of the two integrated stages.	43
3.5	Simulation results of (a) gain (S_{21}) after two stage integration, and (b) 1 dB compression point of the two integrated stages.	44
3.6	Schematic of the Gilbert-cell active mixer.	44
3.7	(a) Schematic of the proposed LNA, (b) Conventional inductive degenerative LNA [8].	47
3.8	Variation (a) of gain (A_{v1}) at gate of the LNA for different values of L_g , (b) of input matching (S_{11}) for different values of L_g , and (c) in NF of IDL-stage for different values of L_g	48
3.9	(a) Complete schematic of the proposed LNA with constant- g_m [10] and biasing circuit, (b) balanced mixer on top of LNA without biasing.	50
3.10	Simulated (a) S_{11} of the proposed LNA across all corners, (b) S_{21} of the proposed LNA across all corners, and (c) NF of the proposed LNA across all corners.	51

3.11	Simulated (a) IIP-3 of the proposed LNA, (b) IIP-2 of the proposed LNA, and (c) Gain and phase mismatch.	53
3.12	(a) Downconverted 900 MHz RF input to 25 MHz, (b) Input matching with mixer on top, and (c) NF of LNA with mixer on top (RF front-end).	55
4.1	The common LNA topologies, (a) inductor degenerated narrowband LNA [8] and, (b) shunt feedback wideband LNA [11].	60
4.2	Shunt-feedback common-source amplifier with narrow-band matching.	61
4.3	Incremental small signal equivalent of schematic in Fig. 4.2.	62
4.4	Input equivalent network of the circuit.	62
4.5	g_m required for $S_{11}=-10$ dB in wideband LNA of Fig. 4.1(b) and the narrowband matched LNA of Fig. 4.2.	64
4.6	Simulated dependance of S_{11} , at a spot frequency of 900 MHz, on the resistor R in case of (a) wideband LNA of Fig. 4.1(b), and (b) narrowband LNA of Fig. 4.2.	65
4.7	Input equivalent RLC circuit of the proposed LNA.	67
4.8	Simulation results of A_{GS} varying with respect to g_m at 900 MHz, while maintaining S_{11} less than -10 dB.	67
4.9	Resistive shunt-feedback LNA (a) without current-reuse, (b) with current-reuse and, (c) as proposed with current-reuse and narrowband input match.	68
4.10	Simulated NF and LNA power consumption inclusive of bias circuits with respect to g_m . S_{11} is maintained at less than -10 dB at 900 MHz.	69

4.11	Modified LNA with half-cascoded pMOS and buffer as a second stage.	72
4.12	Improved S_{11} with modified half-cascoded LNA.	73
4.13	(a) Supply independent constant- g_m and current biasing circuit [10]. (b) Simulation results of supply independent current biasing for the buffer.	73
4.14	Simulation test bench including modified LNA with package parasitics, ESD protection circuit (shown at RF ports only) and external passive com- ponents.	74
4.15	Micrograph of relevant area of the chip and designed PCB for measurements.	75
4.16	Measurement set-up for the noise figure (black connections) and IIP3 (blue connections).	76
4.17	Measured, (a) pre-zap and post-zap I-V characteristics of the on-chip ESD- diode at the gate (RF input) for a 2.5 kV HBM event, (b) S_{11} of three random samples.	78
4.18	Measured, (a) S_{21} of three random samples, (b) NF of three samples with minimum NF of 0.92 dB at the input-match frequency.	79
4.19	Measured, (a) NF as a function of temperature for sample3 (b) IIP_3 of sample3.	80
5.1	A typical LNA test-bench.	85
5.2	(a) Core LNA as a two-port network. (b) Two planes for an integrated LNA with plane-A as off-chip and plane-B as on-chip plane.	86

5.3	(a) Equivalent circuit of a CCS current buffer without biasing, and (b) equivalent circuit of SF buffer without biasing.	87
5.4	(a) Micrograph of a prototype LNA with SF-buffer, (b) measured S_{22} of the LNA with SF, and (c) measured S_{21} of the LNA with SF.	92
5.5	Measured S_{21} and calculated gain using Eq.(5.1).	94
6.1	Switched LNA-Oscillator hybrid circuit with output buffer and auxiliary power amplifier.	99
6.2	Schematic of switched LNA/OSC based Transmitter.	99
6.3	Simulated Phase Noise of 2.4 GHz Oscillator.	100
6.4	Die-micrograph of the switched LNA/OSC hybrid circuit.	100
6.5	Measured power spectrum of the oscillator with a maximum power of -10 dBm at the center frequency of 2.277 GHz.	101
6.6	Power spectrum showing the difference in power at the center frequency and at the offset of 3 MHz.	102
6.7	Measured, (a) FSK spectrum with peak power of -15.8 dBm at 2.369 GHz, and (b) FSK spectrum with the deviation $\Delta F = 108$ MHz.	103
6.8	Measured modulation index (m) variations with (a) deviation $\Delta F = 44.6$ MHz and $m = 45$ with 0 to 0.7 V swing at varactors, and (b) maximum deviation $\Delta F = 139$ MHz and maximum $m = 139$ with rail-to-rail swing at varactors .	104
6.9	Measured OOK spectrum with data rate of 2Mbps (1 MHz clock).	105

6.10	Equivalent schematic during the LNA mode of operation of the hybrid circuit.	106
6.11	Simulated NF and S11 of hybrid circuit in LNA mode.	107
6.12	Simulated S_{21} during the LNA mode of the hybrid circuit.	107
6.13	Measured input matching (S_{11}) of the LNA.	108
6.14	Schematic for debugging the unwanted diode between LNA/OSC switch and LNA input.	109
6.15	I-V characteristics with positive terminal of supply at LNA input and negative at SWITCH.	110
6.16	I-V characteristics with negative terminal of supply at LNA input and positive at SWITCH.	110
6.17	Measured S_{21} with buffer always on and when (a) LNA is turned on, (b) when turned off and, (c) the difference between the two which signifies LNA is giving gain.	111
6.18	Architecture of switched LNA/OSC based Receiver (Initially planned). . .	111
6.19	Proposed on-chip LNA/OSC based receiver's demodulation circuit with a RC LPF and a level shifter for SoC implementation.	112
6.20	Frequency plot of FSK with carriers at -30 dBm modulated by the data at 1 Mbps rate.	113
6.21	Downconverted FSK signal with a 2.4 GHz LO to its baseband signal. . . .	113
6.22	Level shifted FSK demodulated data.	114

6.23	Original data recovered form the FSK signal.	115
6.24	OOK modulated data given to the receiver (in LNA mode). The 2.4 GHz arrier has a power of -21 dBm carrier which is modulated by the 4 Mbps data rate.	115
6.25	Demodulated OOK after the 1 st -order RC LPF.	116
6.26	Level shifted OOK demodulated output.	117
6.27	Recovered digital data after OOK demodulation.	118
7.1	Simulink model of the proposed code based frequency detection hetero- dyne transceiver.	120
7.2	Die micrograph of the twisted shape inductor (left) with floating substrate shield and spiral shape inductor (right) with ground-signal-ground (GSG) pads.	121
7.3	(a) Complete schematic of the proposed LNA with constant- g_m [10] and biasing circuit, (b) balanced mixer on top of LNA without biasng.	122
7.4	Micrograph of relevant area of the chip and designed PCB for measurements.	122
7.5	Micrograph of a prototype LNA with SF-buffer,	123
7.6	Die-micrograph of the switched LNA/OSC hybrid circuit.	124
7.7	Measured power spectrum of the continuous carrier of the transmitter at T-1 and the carrier of the transmitter at T-2, which is phase-locked to T-1 with a 10 Hz frequency offset.	124

7.8	Implemented system diagram for driving phase-shifter to achieve beam-forming.	125
7.9	Designed PCB for driving the RC-phase shifter.	126
7.10	Measured 0-degrees phase response of the RC-phase shifter.	127
7.11	Measured beamformed power spectrum achieving 0-ppm offset with 4 dB power boosted.	128

List of Tables

1.1	Proposed link budget for the transceiver.	4
1.2	Receiver components specifications.	9
1.3	Band pass filter (BPF) specifications.	10
1.4	Low pass filter (LPF-1) specifications.	11
1.5	Specifications of the low pass filter (LPF-2) used as an enveloped detector.	11
1.6	Clock and data recovery circuit specifications.	12
3.1	Simulated inductor-degenerated LNA specifications.	42
3.2	Mixer general specifications from the simulation.	45
3.3	Isolation properties of the Gilbert-cell mixer from simulations.	45
3.4	Component values and device dimensions used in LNA.	55
3.5	Comparison with other state-of-art LNAs.	57
4.1	Comparison with other state-of-art LNAs.	81
5.1	LNA output impedance matching schemes used in previous works.	84

5.2	Improved NF's of the reported LNA's with CCS and output mismatch ($A = 10$).	89
5.3	Improved NF's of the reported LNA's with SF and output mismatch ($A = 10$).	91
5.4	Measured NF, S_{22} and voltage gain of the LNA test-bench with output impedance matched and mismatched.	95

List of Abbreviations

WSN	Wireless Sensor Networks
PLL	Phase Lock Loop
OOK	On-OFF Keying
ASK	Amplitude Shift Keying
Mbps	Mega Bits Per Second
P_r	Received Power
P_t	Transmitted Power
Tx	Transmitter
Rx	Receiver
ED	Envelope Detector
CDR	Clock and Data Recovery
BPF	Band Pass Filter
LNA	Low Noise Amplifier
SRO	Super Regenerative Oscillator
VCO	Voltage Controlled Oscillator
DCO	Digitally Controlled Oscillator
MUX	Multiplexer
PA	Power Amplifier

LPF	Low Pass Filter
SPDT	Single Pole Double Throw
AGC	Automatic Gain Control
LO	Local Oscillator
PD	Phase Detector
CMOS	Complementary Metal Oxide Semiconductor
RF	Radio Frequency
SRF	Self Resonating Frequency
IIP3	Third Order Input Intercept Point
IIP2	Second Order Input Intercept Point
CMOS	Complementary Metal Oxide Semiconductor
NF	Noise Figure
SNR	Signal to Noise Ratio
IF	Intermediate Frequency
IDL	Inductor Degenerated Low noise amplifier
SPICE	Simulation Program with Integrated Circuit Emphasis
SiGe	Silicon-Germanium
AC	Alternating Current
DC	Direct Current
<i>Q</i>	Quality-factor
ESD	Electro Static Discharge

QFN	Quad-Flat No-leads
DUT	Design Under Test
PCB	Printed Circuit Boards
CCS	Cascoded Common Source
SF	Source Follower
ENR	Excess Noise Ratio
HBM	Human Body Model
FSK	Frequency Shift Keying
OSC	Oscillator
FM	Frequency Modulation
